MAX-PLANCK-INSTITUT FÜR PLASMAPHYSIK
GARCHING BEI MÜNCHEN

Thermal stability and erosion of the silicon doped CFC material NS31

Thermische Stabilität und Erosionsverhalten
des Silizium dotierten CFC Materials NS31

Martin Balden

IPP9/112 February 1997

Die nachstehende Arbeit wurde im Rahmen des Vertrages zwischen dem Max-Planck-Institut für Plasmaphysik und der Europäischen Atomgemeinschaft über die Zusammenarbeit auf dem Gebiet der Plasmaphysik durchgeführt.

IPP9/112 Martin Balden Thermal stability and erosion of the silicon doped CFC material NS31

February 1997

Abstract

In the framework of the collaboration with NET/ITER the 3D silicon doped CFC material NS31 with an optimized thermal conductivity was investigated. NS31 is a candidate for the plasma facing material in fusion devices. The sense of the dopant is to decrease the chemical erosion yield and the tritium retention of graphite.

In order to get a view of the morphology scanning electron microscopy (SEM) was used. The distribution and thermal stability of the silicon were controlled using backscattering spectroscopy (BS). Information about the erosion were obtained out of weight loss and CD_4 production measurements regarding monoenergetic deuterium ions.

The material consists of areas of pure graphite, of Si covered fasers, and of Si or SiC crystallites. The areas cover about 0.01-1 mm^2. Inside the BS information depth (~20 µm) the Si distribution is homogeneous, but the Si concentration varies drastically with the lateral position of the analysing spot (~1 mm^2) around the average value of 8-10 at.%.

Due to heating to 1800 K for 2 hours the initial material looses 1-5 % of its mass and SiC crystallites of a few µm size are created everywhere on the surface. Investigations of the Si distribution of heated samples show a depletion zone at the surface (<1 µm) followed by an enrichment layer (6-8 µm). Deep inside the samples the average Si concentration of the initial material is restored. The average over the distribution of the crystallites of µm size and the well known depletion at the surface of the element with the lower sublimation temperature produce the shape of the observed profiles.

Due to a second heating a cut face of a preheated sample does not show a Si enrichment layer, but the depletion layer is produced due to the evaporation of silicon. The mass loss during a second heating could be neglected.

For both chemical erosion processes, the thermally activated hydrocarbon emission (Y_{therm}) and the kinetic ejection of surface hydrocarbon complexes from a collisional energy transfer (Y_{surf}), the chemical erosion is reduced compared to graphite for initial and heated samples. NS31 behave as expected with the sputtering yield somewhere between the yield of graphite and silicon carbide depending on the Si concentration of the individual surface. The highest reduction of the yield was found for a heated sample: a factor 2 at 40 eV and room temperature and a factor 3 at 1 keV and 800 K. Preliminary implantation and thermal desorption measurements do not point out changes in the implantation and trapping behaviour.

IPP9/112 Martin Balden Thermische Stabilität und Erosionsverhalten des Silizium dotierten CFC Materials NS31

Februar 1997

Zusammenfassung

Im Rahmen einer Zusammenarbeit mit NET/ITER wurde das auf Wärmeleitfähigkeit optimierte, Silizium dotierte 3D CFC Material untersucht. NS31 ist ein Kandidat für das Wandmaterial in Plasmamaschinen. Die Dotierung soll unter anderem die chemische Erosion und das Tritiumrückhaltevermögen verglichen zu Graphit reduzieren.

Die Oberflächenmorphologie wurde mittels Rasterelektronenmikroskopie (SEM) studiert. Die Siliziumverteilung sowie deren thermische Stabilität wurde mit Rückstreuspektrometrie (BS) kontrolliert. Informationen über das Erosionsverhalten bezüglich monoenergetischer Deuteriumionen wurden aus Messungen des Gewichtsverlustes und der Methanproduktion (CD_4) gewonnen.

Das Material besteht aus reinem Graphit, aus Silizium ummantelten Graphitfasern und aus Si- oder SiC-Kristallen. Die Bestandteile bedecken an der Oberfläche zwischen ca. 0,01-1 mm^2. Innerhalb der BS-Informationstiefe von ca. 20 µm ist die Siliziumverteilung homogen, variiert aber stark mit der lateralen Position des Analyseflecks (ca. 1 mm^2) um den Mittelwert von 8 bis 10 at.%.

Während des Heizens auf 1800 K für 2 Stunden verliert das Ausgangsmaterial zwischen 1 und 5 % an Masse. Es bilden sich überall auf der Oberfläche kleine SiC-Kristallite im µm-Bereich. Die Untersuchung der Siliziumverteilung der geheizten Proben zeigt eine dünne Verarmungszone (<1 µm) an der Oberfläche, darunter eine Anreicherungszone (6-8 µm) und im Inneren die mittlere Siliziumkonzentration des Ausgangsmaterials. Integration über die Größenverteilungen der Kristallite und über die bekannte Verarmung des Elements mit der niedrigeren Sublimationstemperatur in der Oberflächenzone reproduziert die Form der beobachteten Siliziumprofile.

Das Heizen einer Schnittfläche einer vorher geheizten Probe führt wieder zu einer Verarmungszone. Es wird aber keine Anreicherungszone gebildet. Der Massenverlust bei einem zweiten Heizvorgang ist vernachlässigbar klein.

Es wurden beide chemischen Erosionsprozeße kontrolliert, die thermisch aktivierte Kohlenwasserstoffemission (Y_{therm}) und die kinetische Ejektion von Kohlenwasserstoffkomplexen der Oberfläche durch Energieübertrag bei Kollisionen (Y_{surf}). Für beide Prozesse ist die chemische Erosion des Ausgangsmaterials und der geheizten Proben verglichen zu Graphit deutlich reduziert. NS31 verhält sich wie erwartet: Die Zerstäubungsausbeute liegt zwischen der Ausbeute von Graphit und Siliziumkarbid abhängig von der Siliziumkonzentration der einzelnen Oberfläche. Die größte Reduktion der Ausbeute wurde für eine geheizte Probe gefunden: Faktor 2 bei 40 eV und Raumtemperatur und Faktor 3 bei 1 keV und 800 K. Einleitende Implantations- und Ausgasexperimente deuten nicht auf Änderungen im Aufsammelverhalten für Deuterium hin.

1 Introduction

Carbon is widely used as plasma facing material and is still a favourite for new fusion machines [1]. For structural hardness and high thermal conductivity, CFC materials were developed. Still problems are the chemical reactivity with hydrogen and the high hydrogen retention.

The aim of this report was to determine the erosion yield by bombardment with deuterium ions and to investigate the influence of a heat treatment (2 hours at 1800 K) on the 3D silicon doped CFC material from the manufacturer SEP (Societe Europeenne de Propulsion, France), called NS31.

The sense of the dopant is to reduce the erosion yield (RES and chemical erosion of hydrogen and oxygen) and the hydrogen retention. Usually a dopant in CFC materials reduces the thermal conductivity drastically. Therefore the thermal conductivity of NS31 was optimized by the manufacturing process. The values specified by SEP are given in table 1. Some more physical properties are listed in table 2.

In the framework of the collaboration with ITER the influence of the dopand on the chemical erosion yield and the dopand stability at elevated temperatures was determined. The silicon distribution of the initial (as received) and heated material (surface and bulk) was investigated by helium and proton backscattering spectroscopy (He-RBS and p-BS). To get a view of the material scanning electron microscope (SEM) studies were carried out. Information about the erosion behaviour were obtained out of weight loss and CD_4 production measurements. Deuterium retention was controlled by thermal desorption spectroscopy (TDS). Chemical surface composition could be obtained from in-situ Auger electron spectroscopy (AES) and ex-situ x-ray photoelectron spectroscopy (XPS).

	thermal diffusivity (10^{-6} m^2/s)			thermal conductivity (W/m K)		
	X	Y	Z	X	Y	Z
RT	200	66	60	304	100	91
1100 K	43	16	14	149	55	48
1300 K	39	15	12	141	54	43

TABLE 1: Thermal diffusivity and conductivity of NS31 as specified by SEP

density	2.0 g/cm^3
silicon concentration	8-10 at. %
porosity	5 %
mean atomic mass	13.3-13.6 u
atomic density	0.9 10^{23} $at./cm^3$

TABLE 2: Physical properties of NS31 as specified by SEP

2 Experimental Details

2.1 Samples and treatments

A block of NS31 was mechanically cut into small plates (usually 12×15×1 mm^3). After cutting they were cleaned in an ultrasonic bath. Some samples were heated in vacuum at 1800 K for 2 hours. For the heat treatment an induction oven was used and the temperature was controlled by an optical pyrometer. Some of the heated samples were cut once more to obtain information on the bulk of heated samples.

The samples are labeled by the direction of the surface normal with respect to the three different values of thermal conductivity (X, Y, Z) and three position in the block (1, 2, m). In the following the analysed surfaces are classified by **i**, **h**, and **c** for initial face (samples cut from the received block before heating), heated face, and face cut after heat treatment, respectively. Table 3 give a list of all used samples. Detailed information about the history of each sample can be obtained from the last column. The cut after heat treatment (**c**) produces a **c**-face and a **h**-face (in, out).

face	name	label	treatments / history of sample
i	ax	X1	**b**
i	ay	Y1	**b**
i	b	X2	**b**, AES, SEM, He
h	c1	X2	**i**, He, **h**, He, **h**, He, **b**, SEM, He, p, **b**
h	c4	X2	**h**, **h**, **b**, SEM, He, p
h **c**	d1	Xm	**h**, **c**, He, XPS, SEM, **h**, He (in) **h**, **c**, XPS, SEM, **h**, He, p (out)
i	e	X2	**b**, SEM, XPS, He
h	f	Y1	**h**, **b**, He, XPS, p
i	g	Y1	**b**, He, XPS, b
h **c**	h1	Ym	**h**, **c**, **b**, He, XPS (in) **h**, **c**, He, p (out)
h **c**	h2	Ym	**h**, **c**, He, p (in) **h**, **c**, He, p (out)
i	j	Z1	**i**, He, p
i	k	Y1	**i**, He, p, **b**
h	l	Y1	**h**, b, He, **b**

TABLE 3: List of used samples. b= ion bombardment (sputtering measured by weight loss and residual gas analysis), He= Rutherford backscattering spectrometry (RBS) with 2.0 MeV ^4He, p= backscattering spectrometry (BS) with 2.5 MeV ^1H, SEM= scanning electron microscopy, XPS= x-ray photoelectron spectroscopy, and AES= Auger electron spectroscopy.

2.2 Scanning electron microscopy

In order to get a view of the surface morphology (SEM) was used [2]. All presented SEM pictures are created by the secondary electrons of a 20 keV electron beam. The penetration depth of a 20 keV-beam is about 1-3 μm. The information depth of the secondary electrons is about a few nm. Coupled with the topographic image from the secondary electrons the electron induced X-ray emission (EIXE) yields information on the composition of the material.

2.3 X-ray photoelectron spectroscopy and Auger electron spectroscopy

In order to obtain information of the chemical state of the silicon and the composition in the surface region ex-situ x-ray photoelectron spectroscopy (XPS) [3] and in-situ Auger electron spectroscopy (AES) [4] were used. In the XPS chamber the possibility of sputter cleaning exists. The information depth of both techniques depends on the material and on the energy of the created electrons. It is usually in the range of a few nm.

2.4 Backscattering spectrometry

The silicon concentration (c_{Si}) and depth profile near the surface was determined with backscattering spectrometry. ^{4}He ions and ^{1}H ions with an energy of 2.0 MeV and 2.5 MeV were used, respectively (He-RBS and p-BS). The ion beam hits the target at normal incidence. The scattering angle was 165°. Usually a fluence of 5 μC and 20 μC was accumulated for a single He-RBS and p-BS spectrum, respectively. The size of the analysing spot was about 0.5-1.5 mm^2. The c_{Si} is evaluated by using the program SIMNRA to simulate the measured spectra by iterating the concentration and depth profile. The fit for He backscattering is good as the cross section will be approximated by the Rutherford cross section, while for protons for both, Si and C, non-Rutherford cross section apply, resulting in a poor fit at larger depths. The c_{Si} used here refer to atomic concentrations as usual in ion beam analysis. The information depths of uniform Si doped graphites are listed in tab. 4. For obtaining a depth scale an atomic density for NS31 of 0.9×10^{23} at./cm^3 was used (tab. 2). Changes in density due to concentration variations are neglected by the transformation from at./cm^2 into μm.

	2.0 MeV ^{4}He			2.5 MeV ^{1}H		
energy of ^{28}Si edge (keV)	1135			2170		
energy of ^{12}C edge (keV)	511			1796		
energy of ^{2}D edge (keV)	-			284		
Si concentration (at.%)	10	25	50	10	25	50
maximal information depth of Si (μm)	1.92	1.71	1.47	27.2	24.4	20.7
information depth of Si signal at C edge (μm)	1.17	1.03	0.90	7.6	6.4	5.6
maximal information depth of C (μm)	0.93	0.81	0.70	22.4	20.3	17.4

TABLE 4: The information depths of 2.0 MeV He-RBS and 2.5 MeV p-BS of uniform Si doped graphites. The depths were obtained by using the program SIMNRA.

2.5 Ion bombardment

The ion beam erosion measurements were performed at the high current ion source for light ions [5]. The ion source was adjusted to produce 6 keV D_3^+ ions. Then these ions were slowed down by biasing the target to three times the chosen impact energy. The bombarded spot has a size of about 0.45 cm^2 and 0.6 cm^2 for 1 keV and below 50 eV, respectively. An ion current of between 50 μA and 100 μA was used. This corresponds to a flux of $1.5\text{-}4.2\times10^{15}$ D$^+$/cm^2/s. Most of the bombardments take place at room temperature; the samples #ax, #ay, #c1, #k, and #l were bombarded at higher temperatures to measure the sputtering yield at 800 K and the chemical erosion in the temperature range between RT and 1100 K. The sputtering yield was determined by measuring the weight loss and the ion current (deposited cargo). Detailed data of all these bombardment experiments are summerized in table 5.

To control the chemical part of erosion the CD_4 production versus the target temperature was monitored and compared to pure carbon (HPG from Union Carbide, maximum set to 0.1). During the bombardment the temperature was increased in steps and held for 6 minutes to ensure steady state conditions. Also degassing experiments after D_3^+ implantation were performed using thermal desorption spectroscopy (TDS) up to 1450 K with about 6 K/s heating speed. Only qualitative information on the trapping energy and the D retention in comparison to pure carbon could be gained.

sample _group	E_{impact} [keV]	T_{target} [K]	Q [C]	Δm [μg]	M [u]	yield [0.01]	fluence [10^{19} at cm^{-2}]	sputtered atoms [10^{19} cm^{-2}]
ax_i	1	800	1.1	39	13.6	8.38	4.58	0.384
		RT	2.3	22		2.21	9.58	0.217
ay_i	1	800	0.8	26	13.6	7.68	3.33	0.256
		RT	2.41	30		2.94	10.0	0.295
c1_h	1	800	1.3	35	x16.7	5.18	5.42	0.280
		RT	1.44	32	x18.5	3.85	6.00	0.484
		RT	0.94	13	x19.3	2.30	3.92	0.555
			s3.68	s80			s15.33	s0.555
f_h	0.04	RT	0.95	13	x12.4	3.55	2.97	0.105
			1.88	23	x13.1	2.99	5.88	0.275
			1.29	12	x14.1	2.13	4.03	0.343
			2.36	20	x14.7	1.86	7.38	0.465
			1.11	7.5	x15.1	1.44	3.47	0.501
			1.02	8.5	x15.3	1.75	3.19	0.551
			2.14	17	x15.5	1.65	6.69	0.654
			s10.75	s101			s33.6	s0.654
f_h	0.02	RT	0.71	4.5	x15.6	1.31	2.22	0.679
			1.41	12	x15.7	1.74	4.41	0.752
			2.3	18.5	x15.8	1.64	7.19	0.865
			2.63	21.5	x15.8	1.66	8.22	0.998
			s17.8	s157.5			s55.6	s0.998
h1_c	0.04	RT	1.08	12.5	13.6	2.73	3.38	0.092
			2.00	23.5		2.78	6.25	0.265
			2.98	33		2.62	9.31	0.509
			s6.06	s69		s2.69	s18.9	s0.509
g_i	0.04	RT	0.85	13	13.6	3.61	2.66	0.096
			2.38	29		2.88	7.43	0.310
			1.0	12		2.83	3.13	0.399
			1.1	11.5		2.47	3.44	0.484
			2.29	19.5		2.01	7.16	0.628
			3.59	42		2.76	11.22	0.938
			0.4	5		2.95	1.25	0.975
			0.8	9		2.66	2.50	1.041
			s12.41	s141		s2.68	s38.8	s1.041
l_h	1	800	1.16	44	x13.8	8.84	4.83	0.427
			2.2	62	x15.4	5.89	9.17	0.924
			1.84	56	x15.5	6.30	7.67	1.397
			s5.2	s162			21.67	s1.397

TABLE 5: List of D_3^+ bombardment experiments: sample and group, impact energy per deuterium atom (E), target temperature (T), deposited charge (Q), weight loss (Δm), mean atomic mass (M), sputtering yield, fluence, and the number of sputtered atoms. The spot size was of about 0.45 cm^2 and 0.6 cm^2 for 1 keV and below 50 eV, respectively. For initial and cut faces a homogeneous c_{Si} of 10 at% was assumed. For the heated faces measured silicon depth profiles were used in determining the sputtering yield. The mean atomic mass (marked with x) and the number of sputtered atoms are calculated from these profiles, too. Numbers labeled with s are the sum of the parameter for one sample.

3 Results

3.1 View of the morphology

The material NS31 is very inhomogeneous on microscopic scale. This is good illustrated by the SEM picture shown in figure 1. The sample looks like a marble cake (fig. 1a). The surface can be charaterized by four different areas: (i) big areas of pure graphite, (ii) small areas of big crystallites (30 µm) of Si or SiC, (iii) thin cut carbon fibres (6 µm ∅), and (iv) thick carbon fibres (30 µm ∅) with a smooth coating of Si or SiC, which are best visible in holes due to the production (fig. 1b-e).

After ion bombardment strong erosion profiles are created at the graphite areas (i), the Si or SiC crystallites are rounded (ii), and everywhere on the thick Si or SiC covered fibres (iv) crystallites (4-8 µm) have been grown (fig. 2).

The heat treatment without ion bombardment produce small crystallites (1-3 µm) on the graphite areas (i). The thick fibres stay smooth. Only sometimes they covered with crystallites (4-8 µm). The areas of big crystallites of Si or SiC (ii) could not be detected. They correspond perhaps to areas with a high density of crystallites (fig. 3).

After additional D_3^+ bombardment the concentration and size (2-5 µm) of the crystallites on the graphite areas were grown (i) (fig. 4). So the differences between the areas (i) and (ii) seem to disappear. The strong erosion profiles at the graphite areas (i) and the rounded Si or SiC crystallites are best visible in figure 4b. Every thick fibre is covered completely with rounded crystallites (4-8 µm, fig. 4c). The thin fibres could not be resolved on heated face. Perhaps they are covered with a lot of small crystallites, such that these areas could not be distinguished from the areas (i / ii).

A freshly cut face of a heated sample looks like an initial face. The four features (i-iv) are clearly visible. The only noticeable change due to the heat treatment is the bumpy coating of the thick fibres (fig. 5).

For the heated surface outside a D_3^+ sputtering spot the height of the silicon EIXE signal decreases with decreasing electron beam energy (20, 10, and 5 keV), while it was constant inside a D_3^+ sputtering spot, as also observed on the initial and cut faces. This indicates that the concentration of the silicon of heated faces increases with the depth (see chapter 3.3).

3.2 Chemical state

It was not possible with XPS to determine the chemical state of the silicon in the outer surface. The maximum of the Si-2p peak of NS31 is always between the position of the Si-2p peak of pure silicon and of silicon crabbed indicating a mixture of different chemical states. The fitting of the measured C-1s and Si-2p peak gives no answer of the ratio of pure Si and SiC. Especially changes due to the heat treatment were not observable.

The silicon AES line changed during the measurement due to oxygen from the residual gas. The inhomogeneity make it impossible to follow the change of the surface composition due to the D_3^+ bombardment.

3.3 Silicon distribution and changes due to heat treatment

3.3.1 Weight loss due to heating

Due to the heating to 1800 K for 2 hours the samples lost between 1 and 5 % of their mass. During a second heat treatment the mass loss is less than 0.1 % of their mass. The evaporated material condensed as a silvery film on the walls of the heating chamber.

3.3.2 Helium Rutherford backscattering spectrometry

Additional to the SEM pictures with EIXE measurements, series of He-RBS spectra at different lateral positions along a line demonstrate the inhomogeneity of the silicon distribution (fig. 6). A comparison with spectra generated by the program SIMNRA (dotted curves) shows the range of variation in the c_{Si}. For comparison of the different sample faces and series, the count rate of channel 150 (828 keV) was used to obtain the c_{Si} for each single spectrum (fig. 7). 828 keV corresponds to a depth of around 0.6 µm. The spread in the c_{Si} for initial faces is nearly the same as for cut ones. Some of the heated faces (f, h2, l) cover a broader range in the c_{Si} and some a smaller range but on a higher concentration level (c1, h1). No significant difference was found between the different orientation of the face refer to high thermal conductivity. For all faces the analysing spot size of about 1 mm^2 did not average out the inhomogeneity in the c_{Si}. Therefore, the average over all measured He-RBS spectra for each analysed face were calculated covering about 10 mm^2 (fig. 6 and 8a-c). Finally, the spectra of different faces were averaged over the group of initial, heated, and cut faces (fig. 8d).

The final average spectra of the initial and cut face are nearly identical (fig. 8d). They look like "normal" He-RBS spectra of a homogeneously mixed two component material. They correspond to a composition of 8 at.% Si and 92 at.% C. The average spectra of the heated samples have a different shape: They cannot be simulated using a constant Si concentration and have to be explained by a change of the c_{Si} with the depth. The Si profile starts with a silicon depletion near the surface and increases then with depth (enrichment layer) as also indicated by the EIXE measurements. For the heated sample #f, which was used in the erosion experiments, the Si profile is shown in figure 9. The correlation between energy and depth is nearly linear.

The sample #d1 was heated a second time to 1800 K for 2 hours. So the cut face is also heated. The average spectrum of that face is include in figure 8b. No enrichment layer occurs, but the depletion layer is again visible. Such a depletion is a well known behaviour of Si doped graphites [6].

3.3.3 Proton backscattering spectrometry

To close the gap between the bulk c_{Si} of about 8 at.% and the c_{Si} in the enrichment layer of around 25 at.%, backscattering measurements with 2.5 MeV protons were done yielding information to depths of about 20 µm. Because of the non-Rutherford cross section the spectra look totally different from the He-RBS spectra: Due to the higher non-Rutherford cross section of carbon, the carbon edge is much higher compared to the silicon edge and the carbon signal decreases with decreasing energy instead of the slow linear increase. In figure 10 a lateral scan over a heated face and average spectra of different faces are presented. As seen in the He-RBS spectra the lateral variation in c_{Si} for heated faces is bigger than for initial ones (see fig. 7) and the spread in the average spectra is comparable. Again, the c_{Si} in the surface zone of heated faces is different than of initial ones. The narrow peak at the carbon edge and the rounded silicon edge corresponds to Si depletion at the surface and to the increasing c_{Si} observed in the He-RBS spectra. The broad bum in the Si signal at about 2000 keV and the

dip in the carbon signal at around 1700 keV characterize the enrichment layer. The thickness of the enrichment layer is about 5-8 μm (Tab. 6). The increase in the c_{Si} near the surface is steep followed by a long range decrease to the bulk/initial value. Changes in the bulk/initial value would be visible in the range of 0 to 400 keV, as a comparison of spectra of pure graphite, pure silicon, homogeneous 20 at.% silicon doped graphite, and NS31 show. In this depth, corresponding to about 20 μm, no compositional change can be found. Due to uncertainties in the non-Rutherford cross section of both, Si and C, no quantitative depth profiles for Si in NS31 could be obtained.

information depth (μm)	1	2	4	6	8	10	12	14	16
Si signal (keV) (10 at.% Si)	2110	2050	1920	1790	1650	1500	1340	1170	980
C signal (keV) (10 at.% Si)	1740	1670	1550	1410	1360	1100	930	730	480
C signal (keV) (30 at.% Si)	1720	1650	1500	1340	1160	970	740	460	40

TABLE 6: The information depths of 2.5 MeV p-BS of an uniform doped graphite (10 at.% Si and 30 at.% Si) of the C and the Si signal. The depth was obtained by using the program SIMNRA.

3.3.4 D_3^+ bombardment

For heated samples the c_{Si} of the sputtered faces change with the fluence of the D_3^+ ions due to the Si profile. In figure 11 the average spectra of a scan inside and outside the D_3^+ sputtering spot of the same face for p-BS and He-RBS are shown. Both spectra outside the bombarded spot show the above discussed enrichment layer of 6-8 μm and depletion layer of less than 1 μm thickness. This face has a very strong depletion of Si as the comparison with the pure graphite spectrum indicate. Therefore, the Si edge in the spectra from outside the D_3^+ sputtering spot shifted to a lower energy. The whole surface layer depleted in Si is sputtered away during bombardment, while the Si enrichment layer is too thick to be removed completely. The average He-RBS spectrum from inside the spot looks like a spectrum of a homogeneously doped sample, because the c_{Si} is almost constant in the information depth of the He ions. The same information could be gained out of p-BS: The narrow peak at the carbon edge is missing in the spectrum from inside the spot.

3.4 Sputtering yield and chemical erosion

Total sputtering yield is measured by weight loss. In general it can be assumed that at high fluences the composition of eroded material is equal to the bulk composition. Before reaching this steady state case, at low fluence, the composition of eroded material could differ from the bulk composition due to the preferential sputtering. So, an altered surface composition could be developed.

Due to the changes in dopant concentration during the heating to depths of about 8 μm, the average mass of eroded material raises with fluence. For the determination of the sputtering yield from the measured data the composition of the sputtered material has to take into account: For initial and cut faces a homogeneous c_{Si} of 10 at.% was assumed for the sputtered material and for the heated faces silicon profiles obtained from He-RBS measurements were used to determine the sputtering yield.

In figure 12 the yield data of table 5 except the data at 20 eV are plotted versus the fluence. The yield at 300 K varies around 0.027. No global trends with fluence are visible in the curves. The slight decrease of the yield with fluence of the heated face of #f is not significant larger than the fluctuations of the initial face of #g. Perhaps the big difference in the data at

800 K of sample #c1 and #l at around 0.5×10^{20} at./cm^2 could be explained by the higher c_{Si} of #c1 (see fig. 8).

To relate the yield of NS31 to the yield of graphite and silicon carbide the data of table 7, the average of the data of table 5, are plotted in figure 13. NS31 behave as expected (compare to SEM pictures): the yield is somewhere between the yield of graphite and silicon carbide depending on c_{Si}. The yield of heated samples is a factor 2 and 3 below the graphite value for 40 eV at 300 K and for 1 keV at 800 K, respectively.

The chemical erosion was investigated by mass analysis of emitted molecules. Figure 14 show the CD_4 production yield versus target temperature as determined by mass spectroscopy during irradiation. The peak around 800 K is due to chemical erosion. All NS31 peaks are lower than the graphite curves and with a small shift to higher temperatures (in contrast to 15 at.% boron doped USB15: shift to lower temperatures). The reduction of the CD_4 production depends on the c_{Si}, as the two curves of #l indicate, and is of the same size, as the reduction in the total yield. The chemical erosion is reduced maximal by a factor 2.

The CD_4 production measurements with 30 eV show only a small bump around 800 K, smaller than for graphite. The start value at 300 K is higher than for 1 keV (fig. 14). Both observation are expected in the picture of chemical erosion of J. Roth and C. Garcia-Rosales [7] (fig. 13). In that picture two processes, the thermally activated hydrocarbon emission (Y_{therm}) and the kinetic ejection of surface hydrocarbon complexes from a collisional energy transfer (Y_{surf}), contribute to the chemical erosion.

In all observation we did not see a significant influence of the direction of high thermal conductivity. For the case of weight loss and CD_4 production measurements a direct comparison of sample #ax and #ay is possible (Tab. 5, Fig. 14).

target	energy	yield
initial and cut, 300 K	40 eV	0.027
heated, 300 K	40 eV	0.017
heated, 300 K	20 eV	0.016
initial, 300 K	1 keV	0.026
initial, 800 K	1 keV	0.08
heated, 800 K,	1 keV	0.06

TABLE 7: Average values of the sputtering yield. The data of table 5 are used.

3.5 Deuterium retention

Figure 15 show the results of TDS measurements after D implantation. The shape of the TDS spectra looks very similar for NS31 and graphite indicating that the trapping energies of D_2 should be the same. A small shift in the peak maximum indicates that the trapping energy of CD_4 is higher for NS31. The retention of D in NS31 did not saturate with fluence. This behaviour is also known form pure graphite [8]. Such a steady increase as in figure 15b is interpreted as the migration of deuterium into the bulk along grain boundaries and trapping beyond the implantation zone [9]. The slope of NS31 is equal or higher than for graphite. It is still unclear, whether the presence of the dopant or the structure increases the slope. Higher slopes have been often observed for different dopants [10].

At low D fluences the formation of CD_4 is not observable. The onset of CD_4 signal occurs rather at fluences where the local D concentration in the implantation zone is high enough to form methane molecules or precursors during implantation and not during subsequent thermal desorption [11].

D retention is also visible in the p-BS spectra of figure 10 and 11 as a small peak around 270 keV, just below the D edge (tab. 4). It is interesting to note, that in the wings of the D_3^+ sputtering spot, where the D fluence was not high enough to sputter away the silicon depletion layer, the deuterium retention is higher than in the centre of the spot. This interesting observation is not investigated in more detail till now. It could be speculated that the saturation concentration in the implantation zone of NS31 is smaller than for graphite (surface of the heated face).

3.6 Silicon profile model

The material NS31 is inhomogeneous in structure and silicon concentration. The received material is unstable at elevated temperatures. The heat treatment produces a Si depletion layer (<1 μm) at the surface followed by a Si enrichment layer (6-8 μm). Till now no model for the creation of enrichment and a depletion layer was found. All simple diffusion or segregation models produces only one, an enrichment or a depletion layer. One possible explanation of the observed silicon profile is the following: During the heat treatment the silicon reaches the surface, more than could evaporate, and crystallises in SiC crystallites. With time these crystallites loose silicon in the surface near region. The average over the distribution of the crystallites of μm size and the depletion of surface produce the observed profile. The maximum silicon concentration in the enrichment layer depends on the reserves of pure silicon in the received material. These reserves could be created during the siliconization of the production process and their distribution should be inhomogeneous. If the reserves exhausts during a heat treatment, a freshly cut face of a preheated sample does not have a Si enrichment layer due to a repeated heating, but still produces the depletion layer due to evaporating of silicon.

4 Conclusion and recommendation

The material NS31 is inhomogeneous in structure and silicon concentration. Due to a heat treatment to 1800 K the initial material looses several percent of its mass and the silicon distribution is changed near the surface dramatically: a Si depletion layer (<1 μm) at the surface followed by a Si enrichment layer (6-8 μm). Due to a second heating a cut face of a preheated sample does not show a Si enrichment layer, but the depletion layer is produced due to the evaporation of silicon. The mass loss during a second heating could be neglected.

For both chemical erosion processes, the thermally activated hydrocarbon emission (Y_{therm}) and the kinetic ejection of surface hydrocarbon complexes from a collisional energy transfer (Y_{surf}), the yield is reduced by a factor around 2 compared to graphite for initial and heated faces. NS31 behave as expected with a sputtering yield somewhere between the yield of graphite and silicon carbide depending on the Si concentration of the individual face.

Before the NS31 is used in fusion machines as plasma facing material, it should be heated to degas and to get a thermal stable material.

Acknowledgements

The author would like to J. Gruber of the Institut Dr. Ing. H. Klingele (SEM), W. Ottenberger (D_3^+ bombardment), H. Plank (XPS, D_3^+ bombardment), and J. Roth (He-RBS) for the experimental performance and assistance. For stimulating and fruitful discussions the author is pleased to acknowledge to C.H. Wu and J. Roth.

Literature

[1] ITER Plasma Facing Components, ITER Documentation Series, No. 30, IAEA, Vienna (1991)
[2] Institut Dr. Ing. H. Klingele, Adelgundenstr. 8, 80538 München.
[3] S. Miller, G.L.P. Berning, H. Plank, J. Roth, submitted to J. Vac. Sci. Technol A.
[4] R. Schwörer, J. Roth, J. Appl. Phys. 77 (1995) 3812.
[5] W. Eckstein, C. Garcia-Rosales, J. Roth, W. Ottenberger, Sputtering Data, Max-Planck-Institut für Plasmaphysik, Report IPP 9/82 (1993).
[6] J. Roth, J. Bohdansky, J.B. Roberto, J. Nucl. Mater. 128&129 (1984) 534.
[7] J. Roth, Garcia-Rosales, Nucl. Fusion, in press.
[8] A.A. Haasz, J.W. Davis, J. Nucl. Mater. 209 (1994) 155.
[9] A.A. Haasz, P. Franzen, J.W. Davis, S. Chiu, C.S. Pitcher, J. Appl. Phys. 77 (1995) 66.
[10] A.A. Haasz, J.W. Davis, J. Nucl. Mater. 232 (1996) 219.
[11] S. Chiu, A.A. Haasz, J. Nucl. Mater. 210 (1994) 34.

Figure captions

FIGURE 1: SEM pictures of the initial face of sample #b before ion bombardment. a) overview; b) on the left: thin carbon fibres; on the right: thick carbon fibres with a smooth coating of Si or SiC; c) area of pure graphite; d) area of big crystallites of Si or SiC; e) thick carbon fibres with a smooth coating of Si or SiC.

FIGURE 2: SEM pictures of the initial face of sample #b after ion bombardment. a) on the right top corner: strong erosion profiles of a pure graphite area; on the left bottom corner: rounded Si or SiC crystallites; b) thick fibres with crystallites of Si or SiC.

FIGURE 3: SEM pictures of a heated sample (#c1) before D_3^+ bombardment. a) graphite areas with small crystallites; b) thick fibres with a Si or SiC cover.

FIGURE 4: SEM pictures of a heated face (#c1) after D_3^+ bombardment. a) crystallites on a graphite area; b) strong erosion profiles at a graphite area and rounded Si or SiC crystallites; c) thick fibres covered with Si or SiC crystallites.

FIGURE 5: SEM pictures of a face cut after heat treatment (#d1). a) left bottom corner: pure graphite area; bright spots at the left top corner and at the right bottom corner: small areas of big crystallites of Si or SiC; middle left: thin carbon fibres; middle right: thick carbon fibres with a bumpy cover of Si or SiC; b) detail: thin carbon fibres; c) detail: thick carbon fibres with a bumpy cover of Si or SiC.

FIGURE 6: Thin lines: 2 MeV He-RBS spectra at different lateral positions along a line of the initial face of sample #k and the heated face of sample #l; thick lines: average over all measured spectra of these faces (more than shown here); dotted lines: series of spectra generated by the program SIMNRA for carbon homogeneously doped with silicon between 0 and 50 at.% in 5 at.% steps. The count rate of channel 150 (828 keV, vertical line) was used to obtain the silicon concentration scale refer to a depth of around 0.6 μm.

FIGURE 7: Silicon concentration at a depth of around 0.6 μm for each single spectrum of the different lateral scans. The silicon concentration was obtained by using a comparison of the count rate of channel 150 (828 keV) and of spectra generated by the program SIMNRA. The names of the samples are labeled.

FIGURE 8: Averaged 2 MeV He-RBS spectra of all measured spectra for the different faces grouped in initial a), cut b), and heated c) faces. Thin lines: average over each different face; thick lines: average spectra over the different faces of each group. The samples are ordered from highest to lowest He-RBS signal at channel 150 (initial: c, b ,g, j, e, k; cut: h1, h2, d1; heated: h1, c1, l, f, d1, h2). For comparison the final average spectra of each group and a generated spectra are presented in d). For the average spectrum of the initial (heated / cut) face 133 (154 / 96) single spectra of 6 (6 / 3) different samples was used. The dotted spectrum is generated by the program SIMNRA for carbon homogeneously doped with 8 at.% silicon.

FIGURE 9: Silicon depth profile (diamonds, left scale) used for the RBS spectrum generated by the program SIMNRA (thick line, right scale) to approximate the average 2 MeV He-RBS spectrum of the heated sample #f (triangles). The insert shows the energy dependence of the depth for this profile (squares) and a linear fit (dashed line).

FIGURE 10: Top: 2.5 MeV p-BS spectra of a lateral scan of #f outside the D_3^+ sputtering spot; bottom: average spectra of different samples. The average spectra are ordered from highest to lowest BS signal at 1700 keV (or from lowest to highest BS signal at 2050 keV). Dots: pure graphite; lines: initial face of sample #j, heated face of the sample #d1, #f, #c4 (inside the D_3^+ sputtering spot), and #h1.

FIGURE 11: Average spectra of a scan inside (solid triangles) and outside (open triangles) the D_3^+ sputtering spot of the heated face of sample #f for 2.5 MeV p-BS (top) and 2.0 MeV He-RBS (bottom). The thin line shows a part of a spectrum of pure graphite.

FIGURE 12: The sputtering yield of different samples with different silicon concentrations versus fluence. Open and solid symbols indicate data gained with impact energy of 40 eV and 1 keV, respectively. The dotted line separated the data at 800 K (above) and 300 K (below). The used samples and the used Si-concentration to determine the yield are indicated in the legend.

FIGURE 13: Sputtering yield data of pure graphite at 300 K (open circles) and at 800 K (solid circles), of SiC (crosses), of the initial faces at 300 K (up triangles) and 800 K (down triangles), and heated faces of NS31 at 300 K (squares) and 800 K (diamonds). The lines are the result of the fit including the chemical erosion of J. Roth and C. Garcia-Rosales [7] to the graphite data.

FIGURE 14: CD_4 production yield versus target temperature. Closed lines: pure graphite at 1 keV and 30 eV D_3^+ bombardment; dashed lines: initial samples #ax, #ay, and #k at 1 keV; dotted lines: initial samples #ax and #ay at 30 eV; circles: heated face before weight loss measurement (open) and after a fluence of 1.4×10^{20} at./cm^2 (solid).

FIGURE 15: Top: TDS spectra of the D_2 QMS signal (circles) and the CD_4 QMS signal (triangles) of pure graphite (open) and sample #k (solid) after an implantation of 1.3×10^{18} at./cm^2; bottom: the integral TDS signal versus the deuterium fluence.

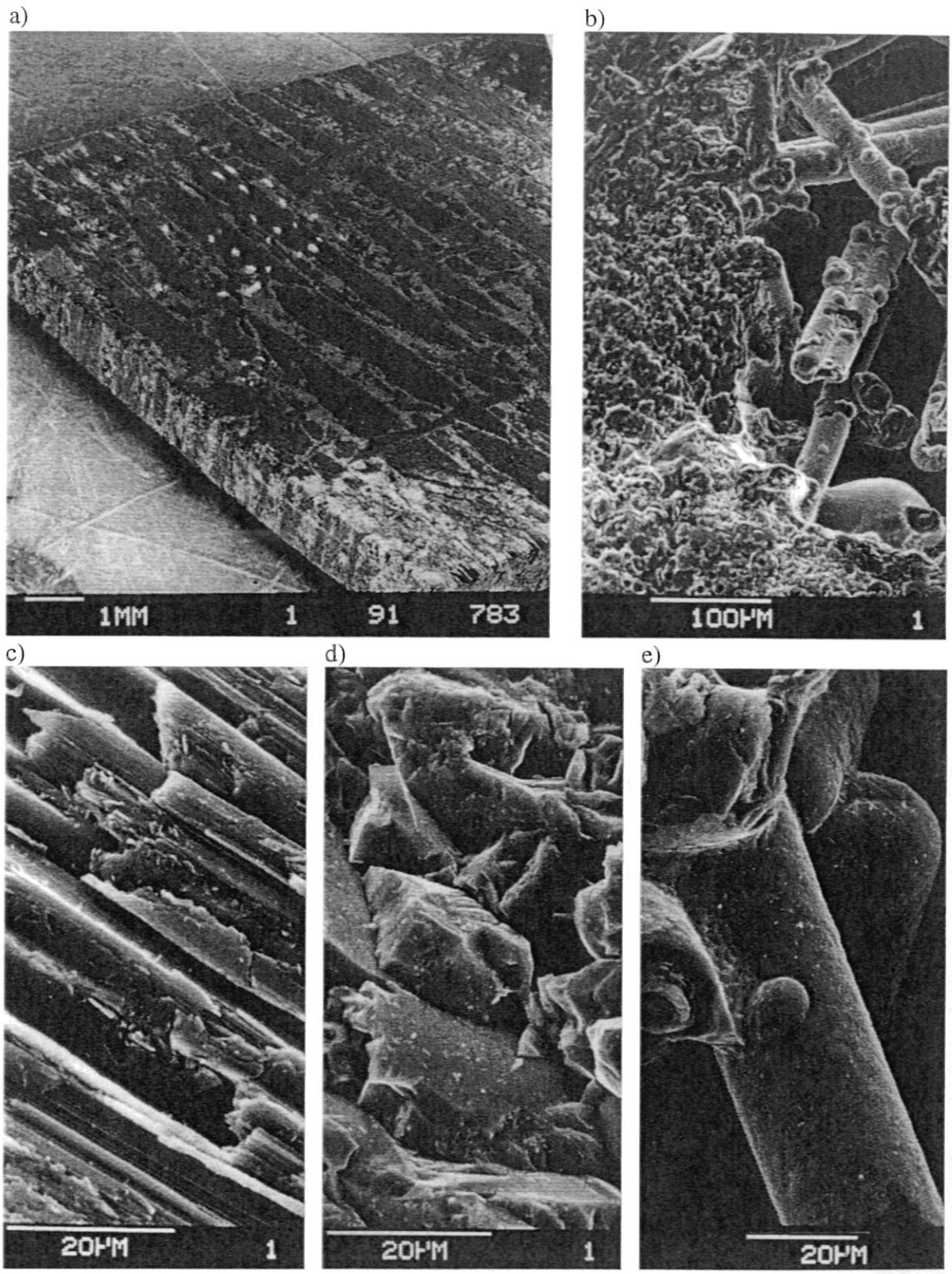

FIGURE 1

a)

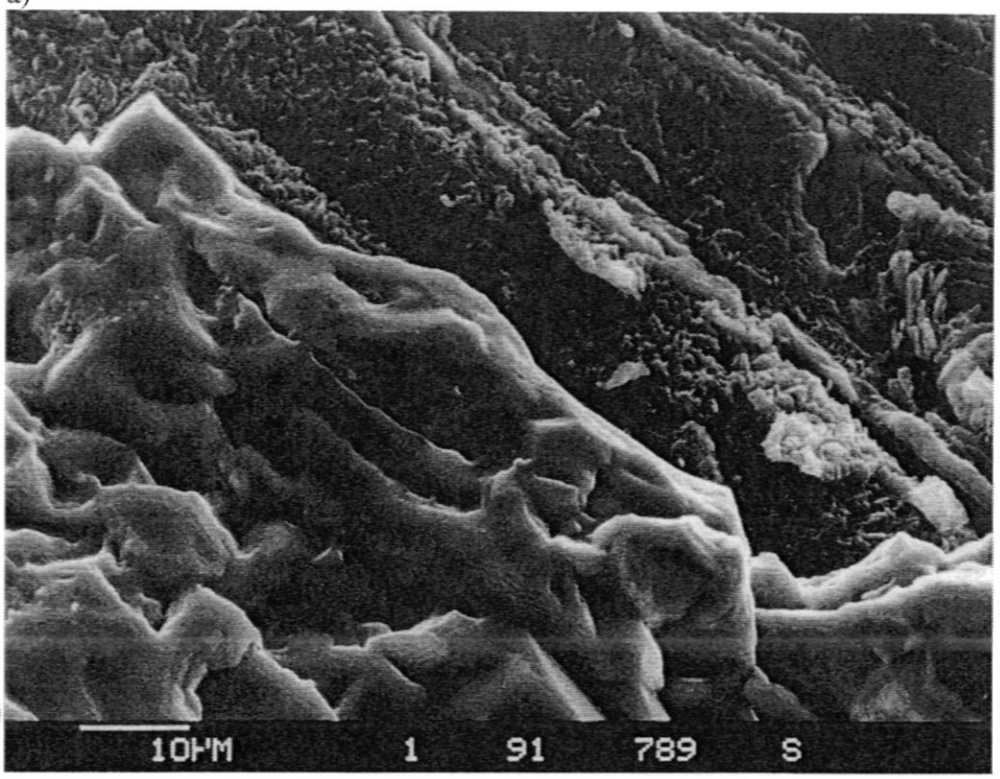

b)

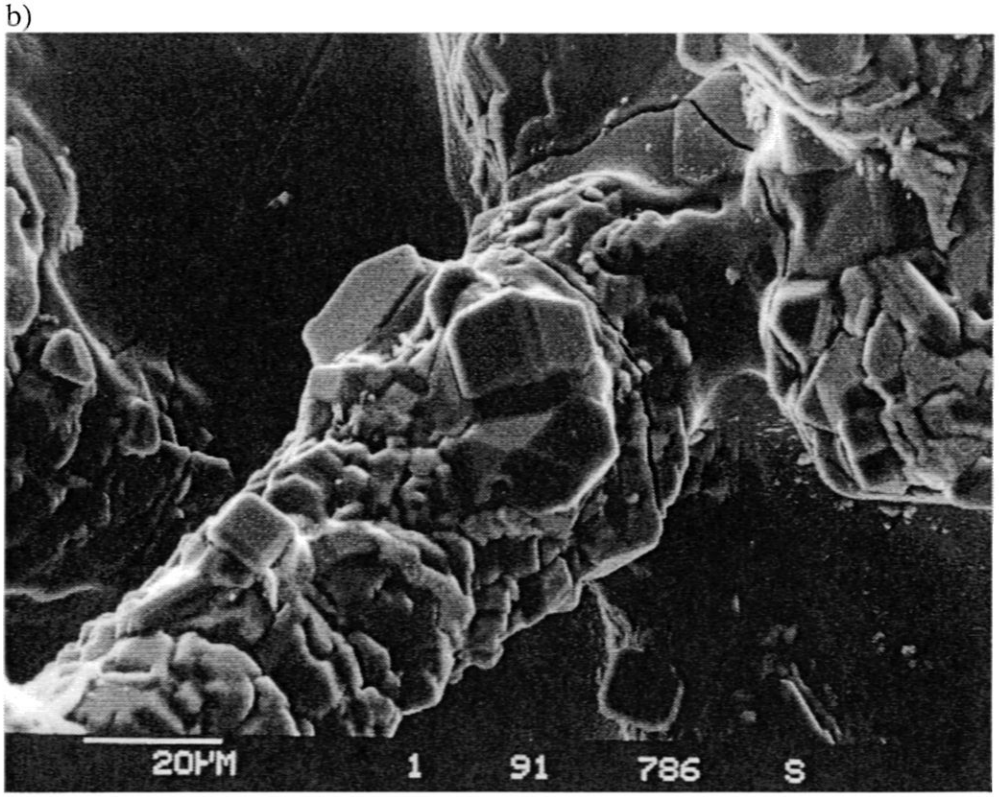

FIGURE 2

a)

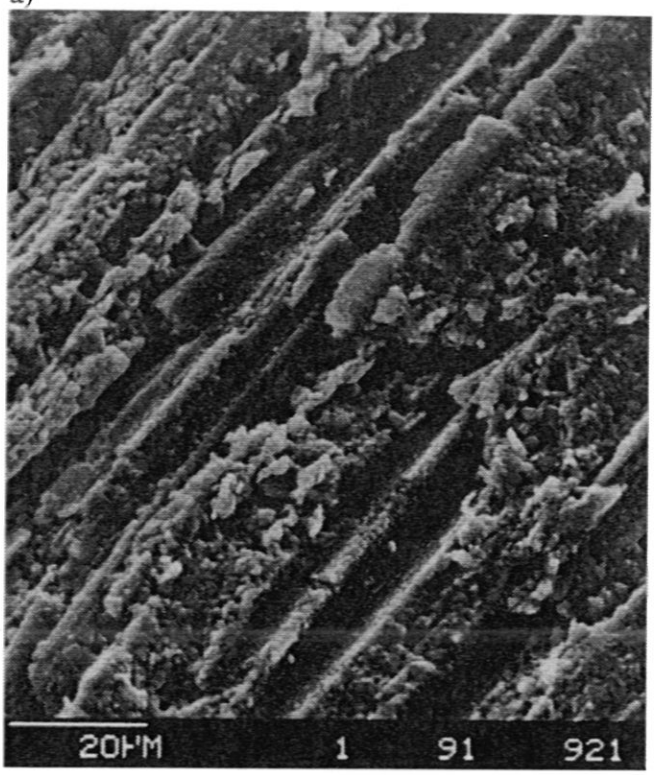

b)

FIGURE 3

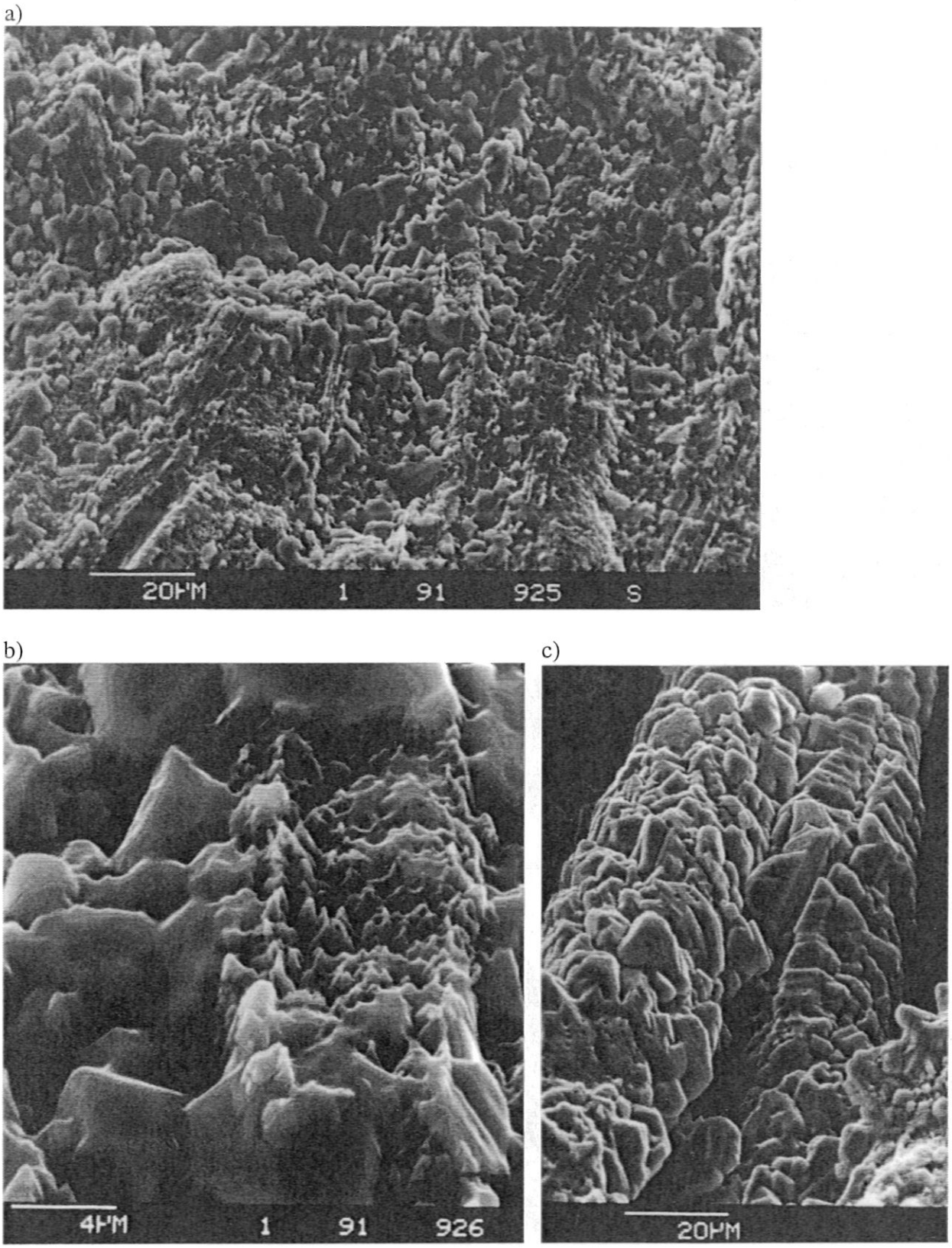

FIGURE 4

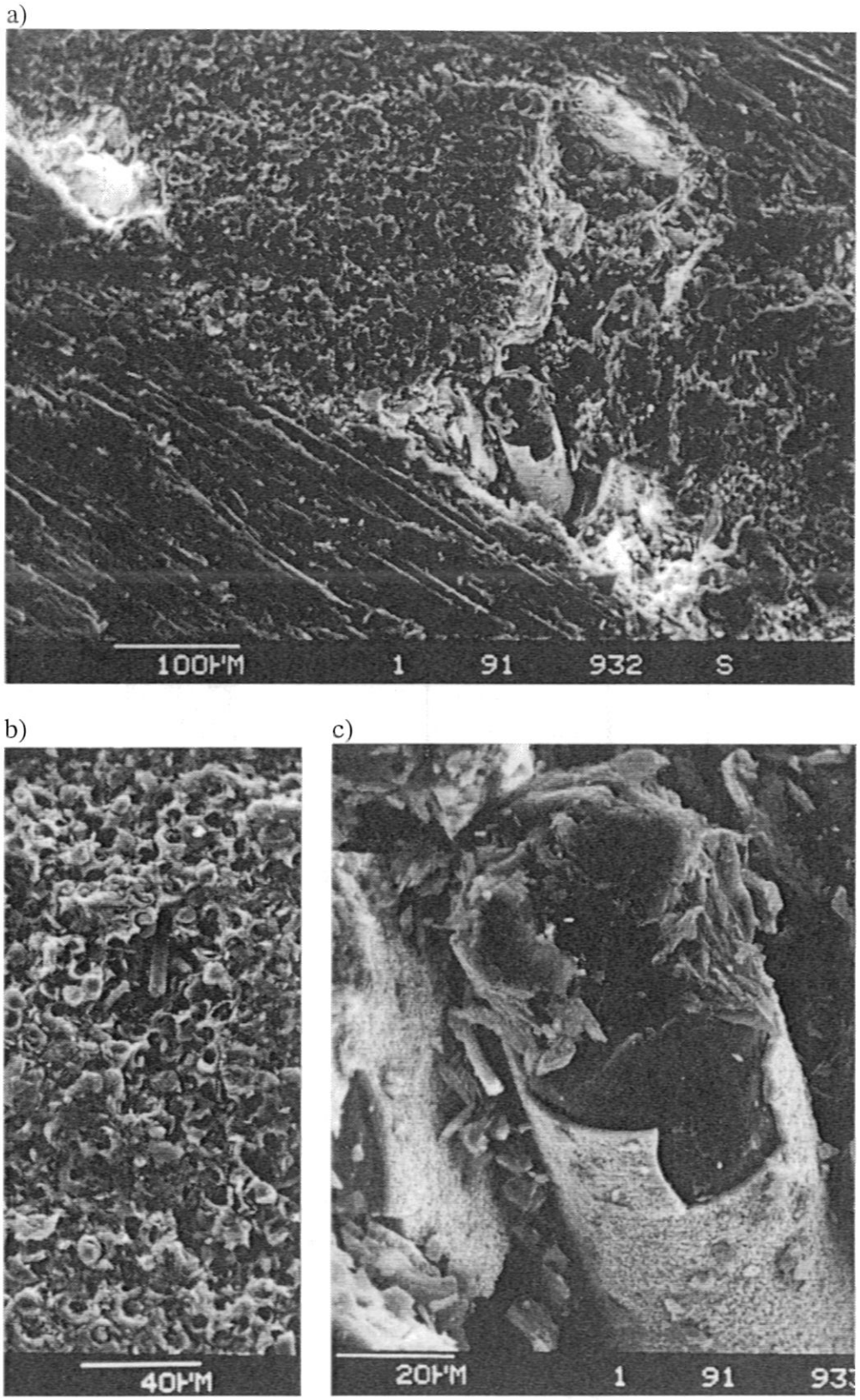

FIGURE 5

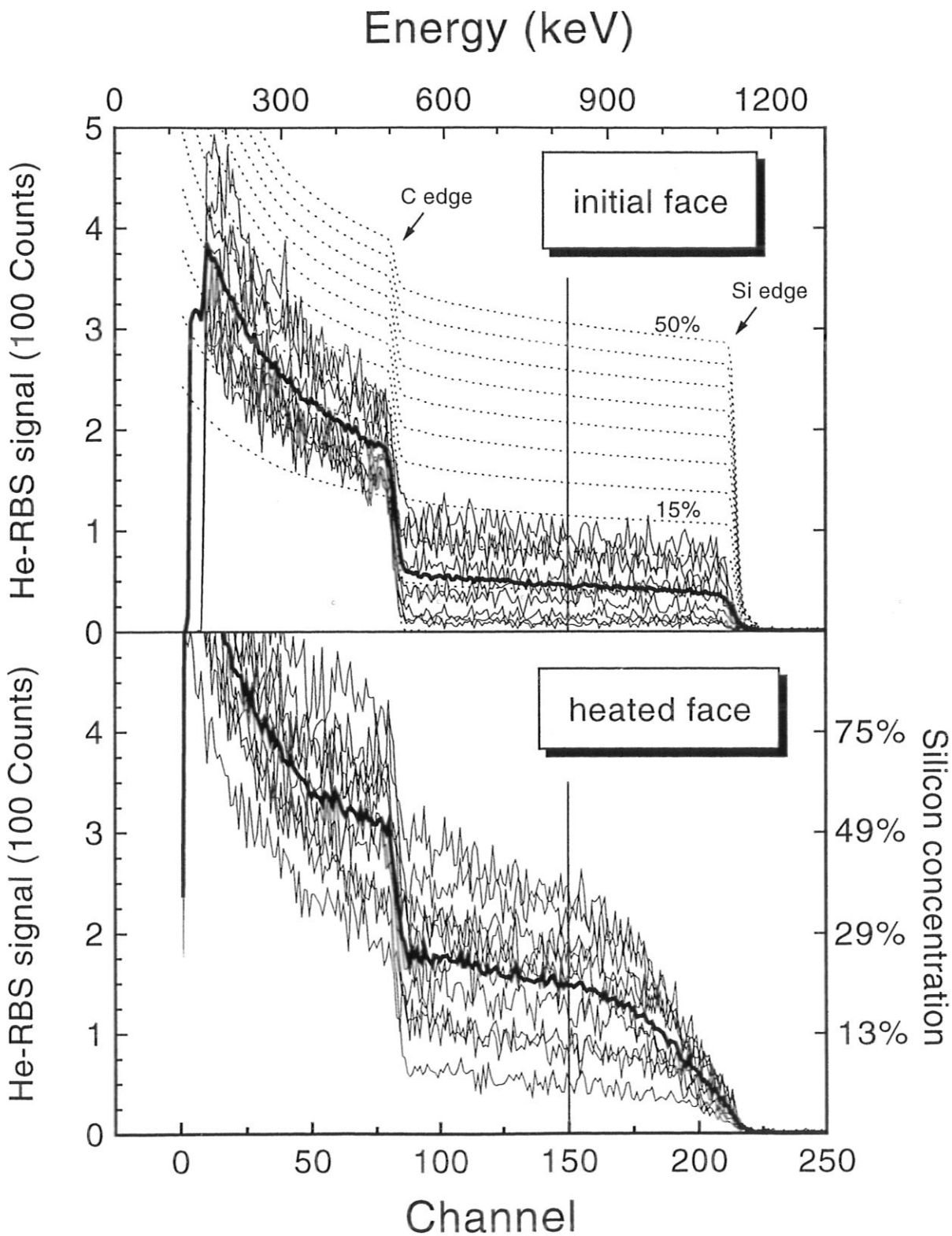
Energy (keV)
0
300
600
900
1200
C edge
initial face
Si edge
50%
15%
heated face
He-RBS signal (100 Counts)
He-RBS signal (100 Counts)
75%
49%
29%
13%
Silicon concentration
0
50
100
150
200
250
Channel

FIGURE 6

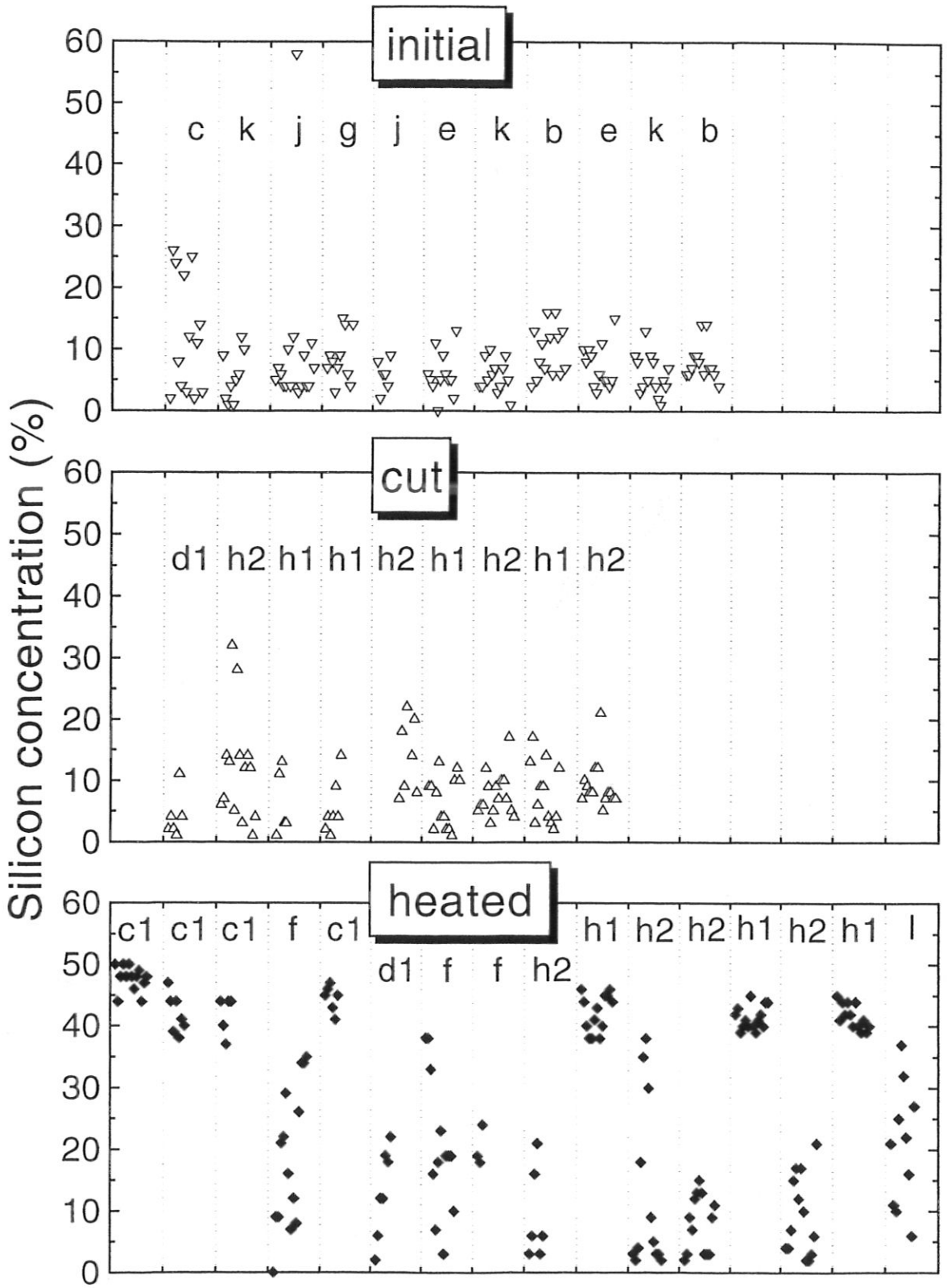
initial
c k j g j e k b e k b
cut
d1 h2 h1 h1 h2 h1 h2 h1 h2
heated
c1 c1 c1 f c1 d1 f f h2 h1 h2 h2 h1 h2 h1 l
Silicon concentration (%)
0
10
20
30
40
50
60

FIGURE 7

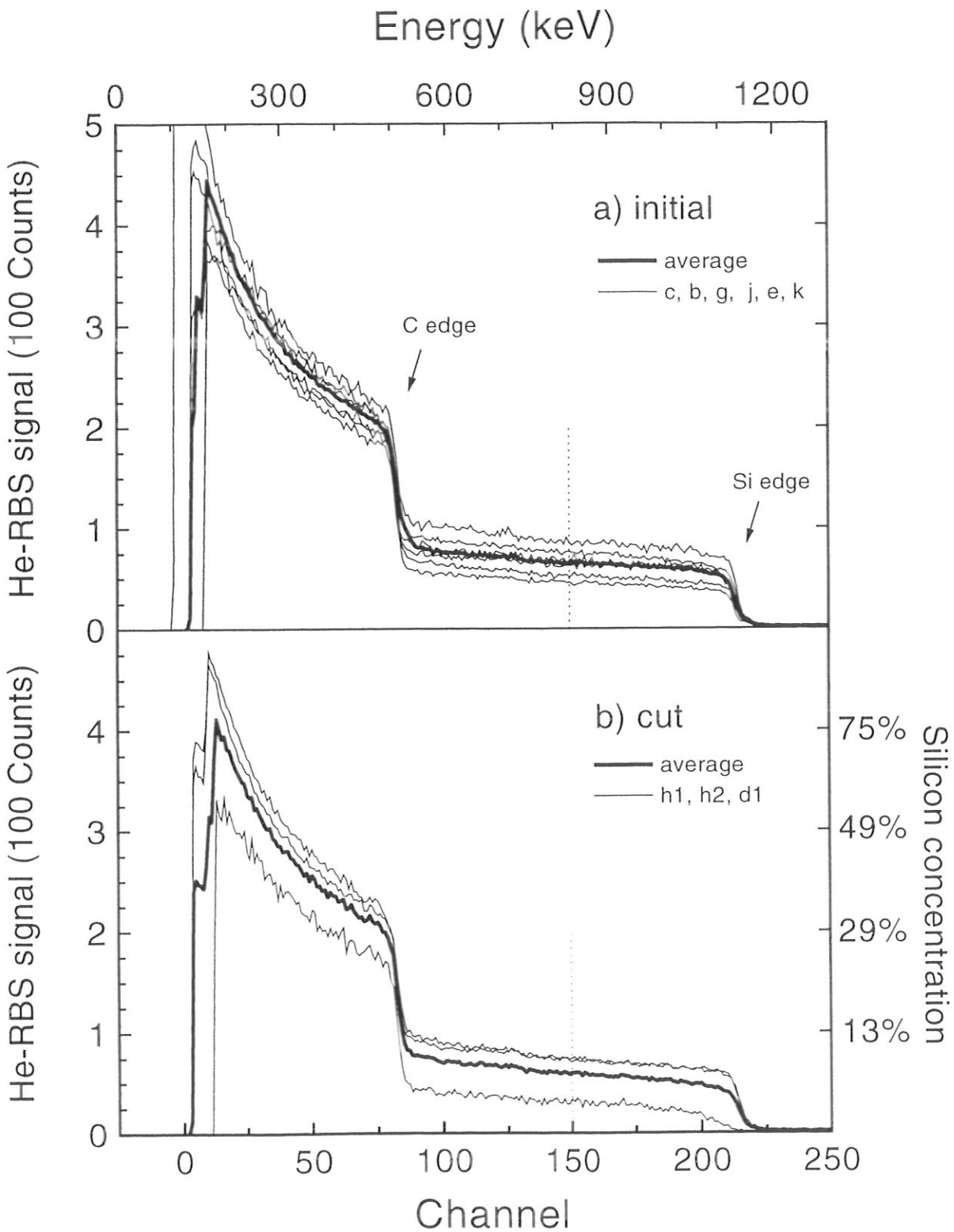

FIGURE 8 (Part a, b)

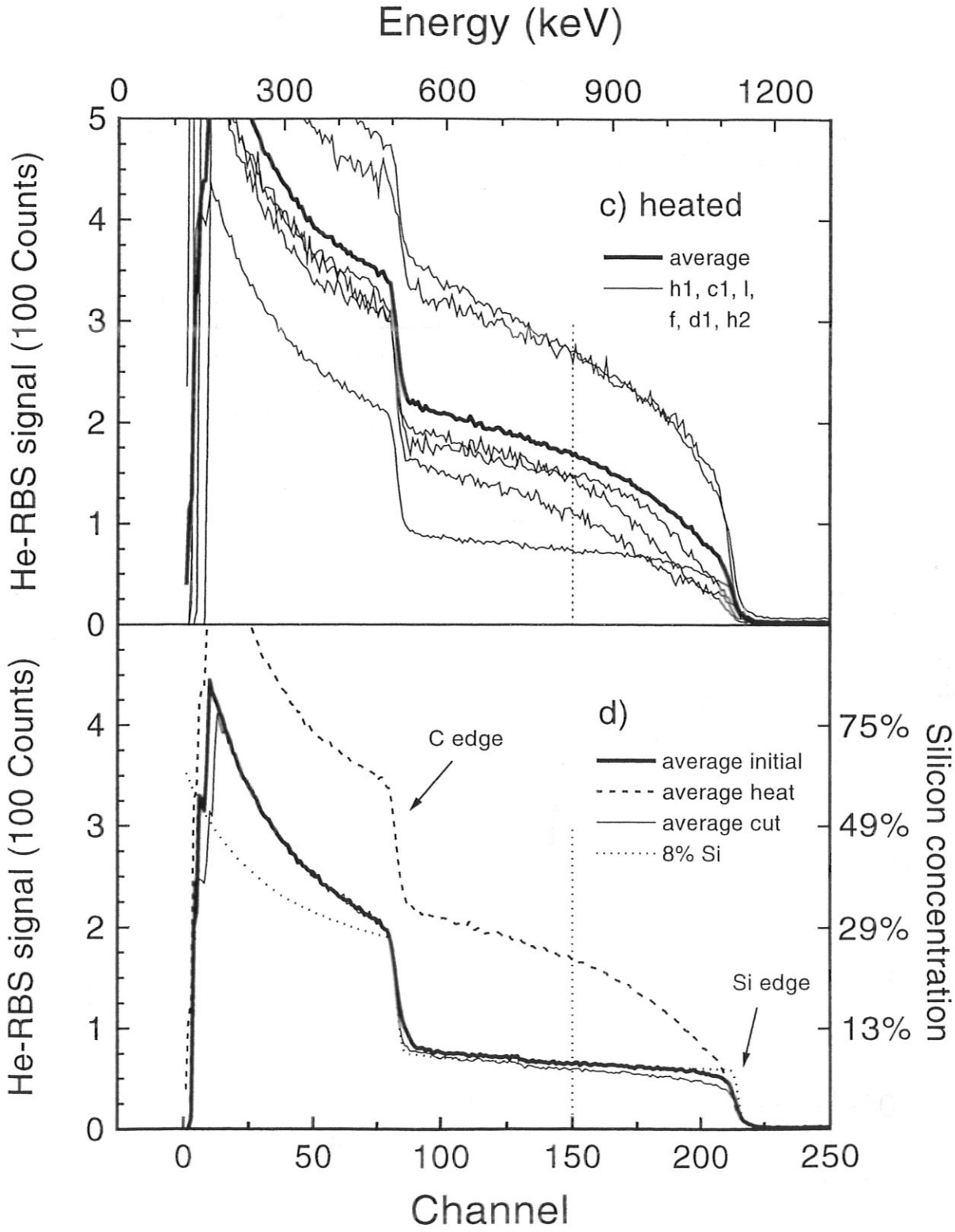

FIGURE 8 (Part c, d)

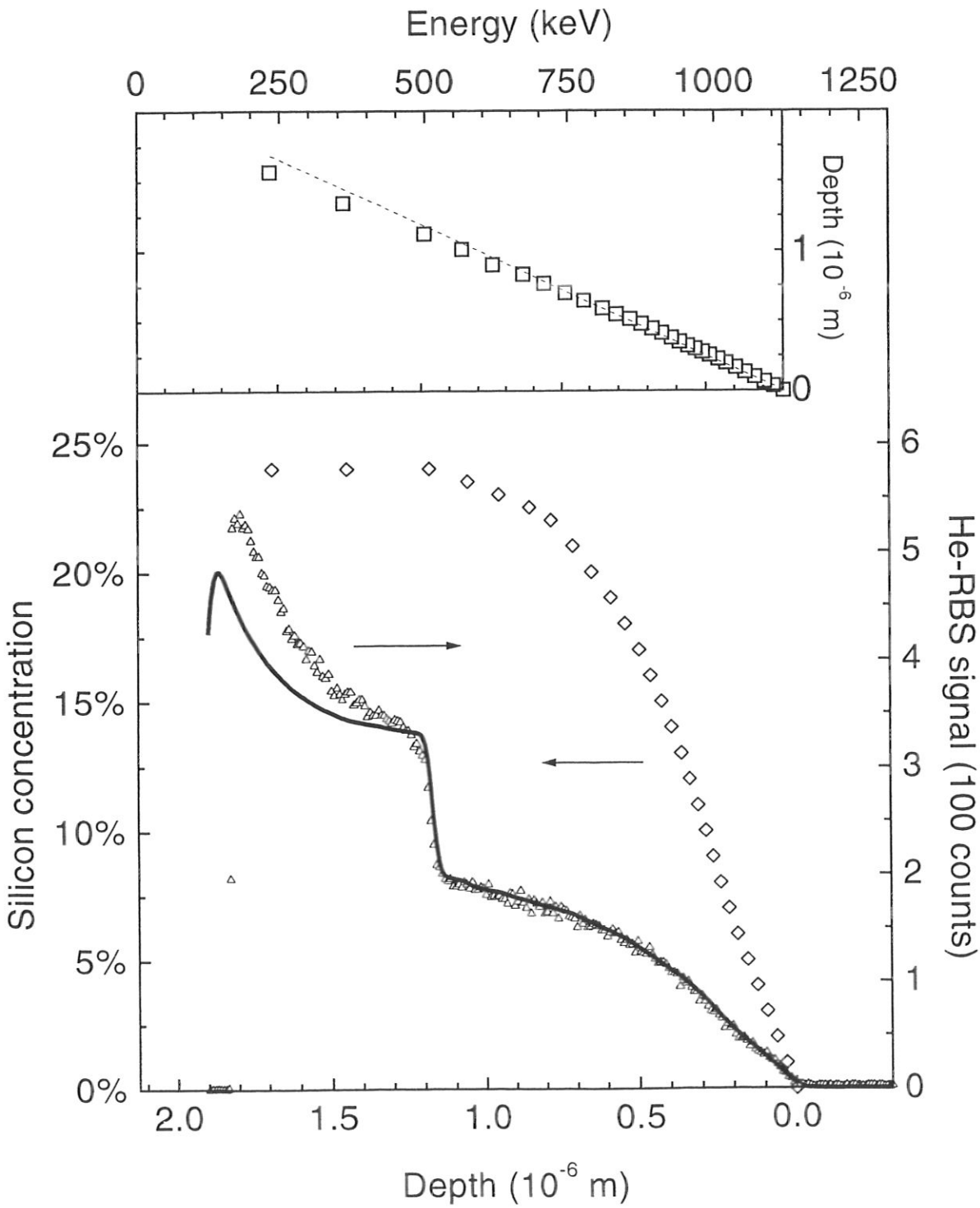
Energy (keV)
0
250
500
750
1000
1250
Depth (10^{-6} m)
1
0
25%
20%
15%
10%
5%
0%
Silicon concentration
6
5
4
3
2
1
0
He-RBS signal (100 counts)
2.0
1.5
1.0
0.5
0.0
Depth (10^{-6} m)

FIGURE 9

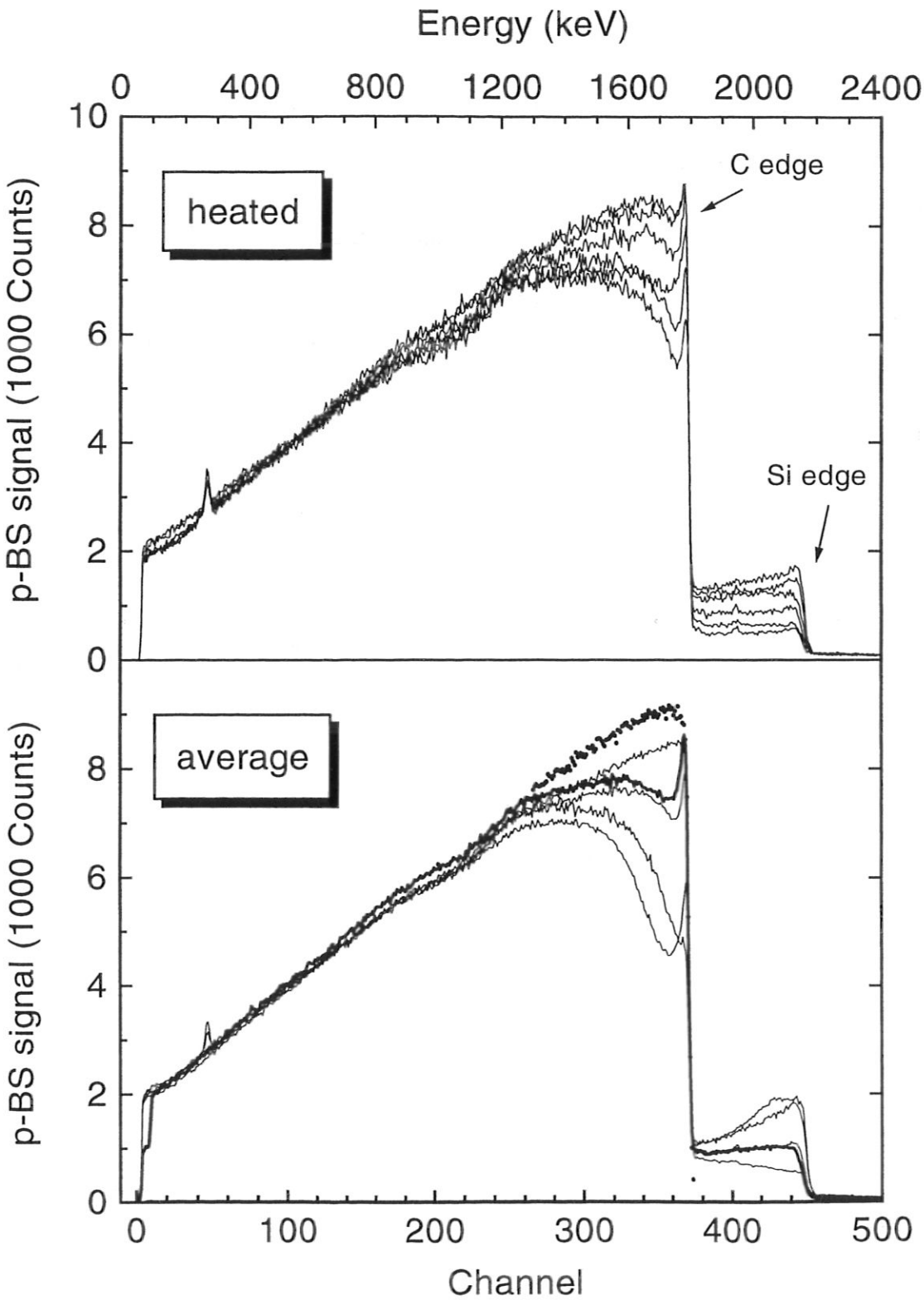
Energy (keV)
0
400
800
1200
1600
2000
2400
heated
C edge
Si edge
p-BS signal (1000 Counts)
10
8
6
4
2
0
average
p-BS signal (1000 Counts)
0
100
200
300
400
500
Channel

FIGURE 10

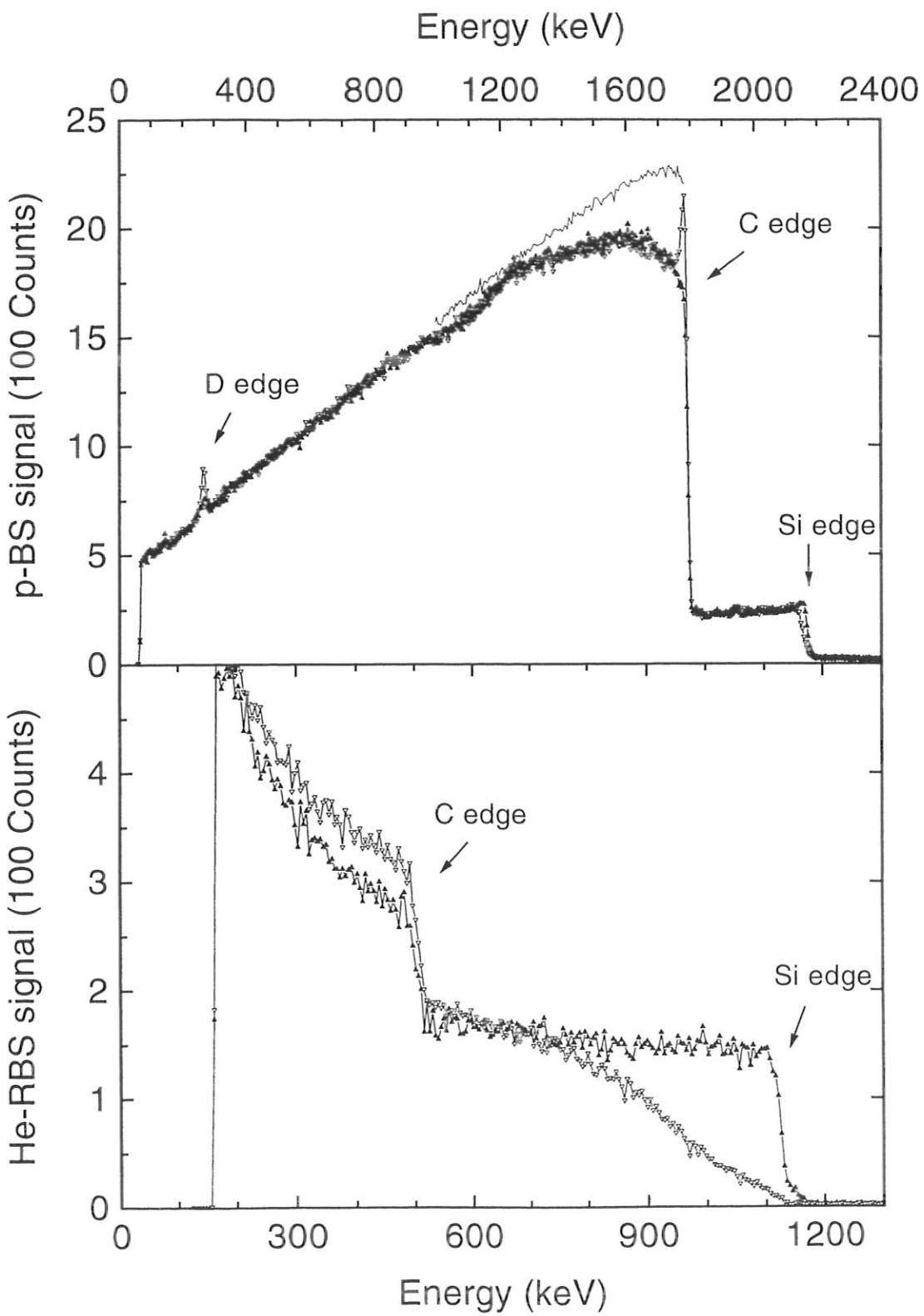
Energy (keV)
0
400
800
1200
1600
2000
2400
25
20
15
10
5
0
p-BS signal (100 Counts)
C edge
D edge
Si edge
He-RBS signal (100 Counts)
4
3
2
1
0
C edge
Si edge
0
300
600
900
1200
Energy (keV)

FIGURE 11

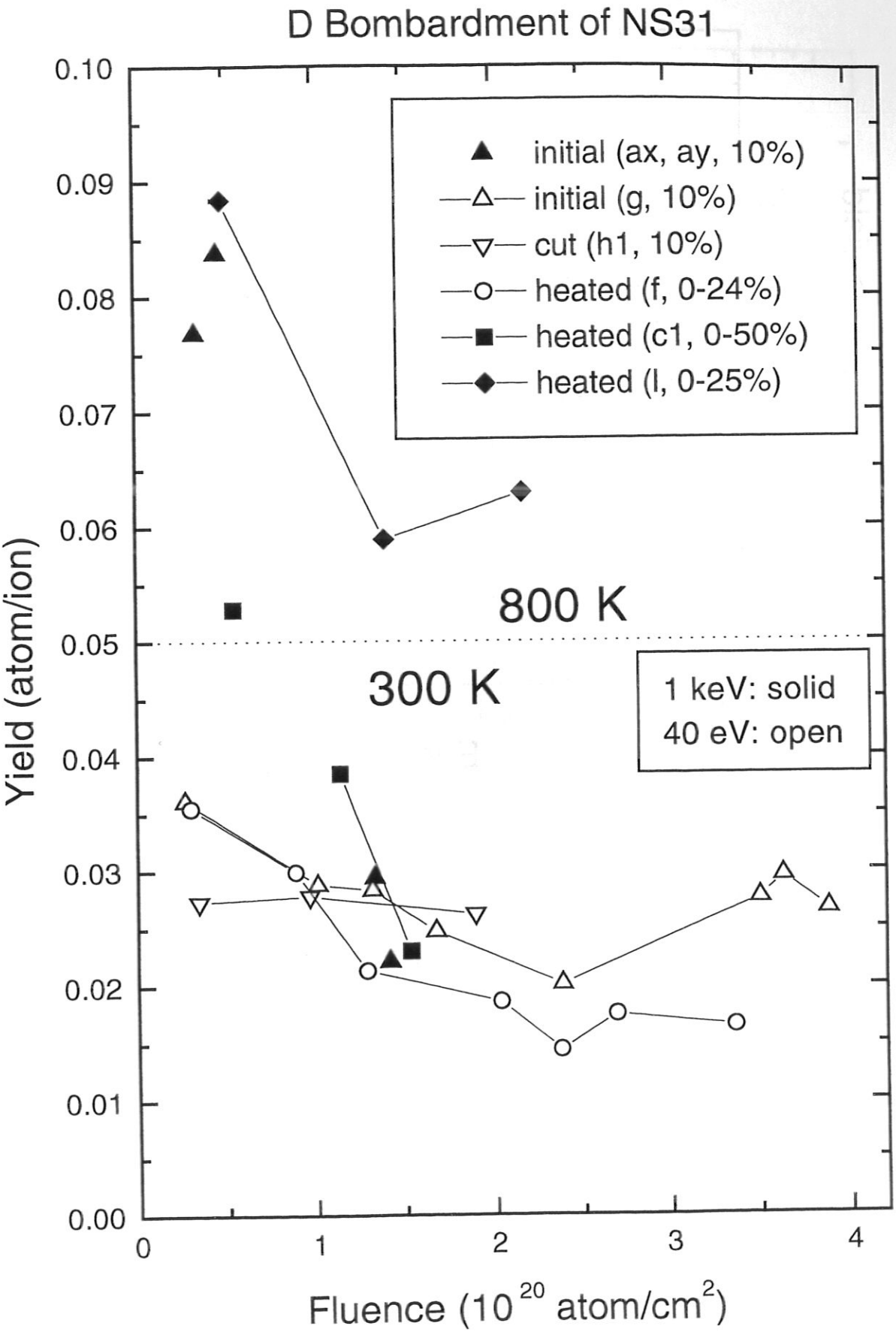
D Bombardment of NS31
initial (ax, ay, 10%)
initial (g, 10%)
cut (h1, 10%)
heated (f, 0-24%)
heated (c1, 0-50%)
heated (l, 0-25%)
800 K
300 K
1 keV: solid
40 eV: open
Yield (atom/ion)
Fluence (10^20 atom/cm^2)
0.10
0.09
0.08
0.07
0.06
0.05
0.04
0.03
0.02
0.01
0.00
0
1
2
3
4

FIGURE 12

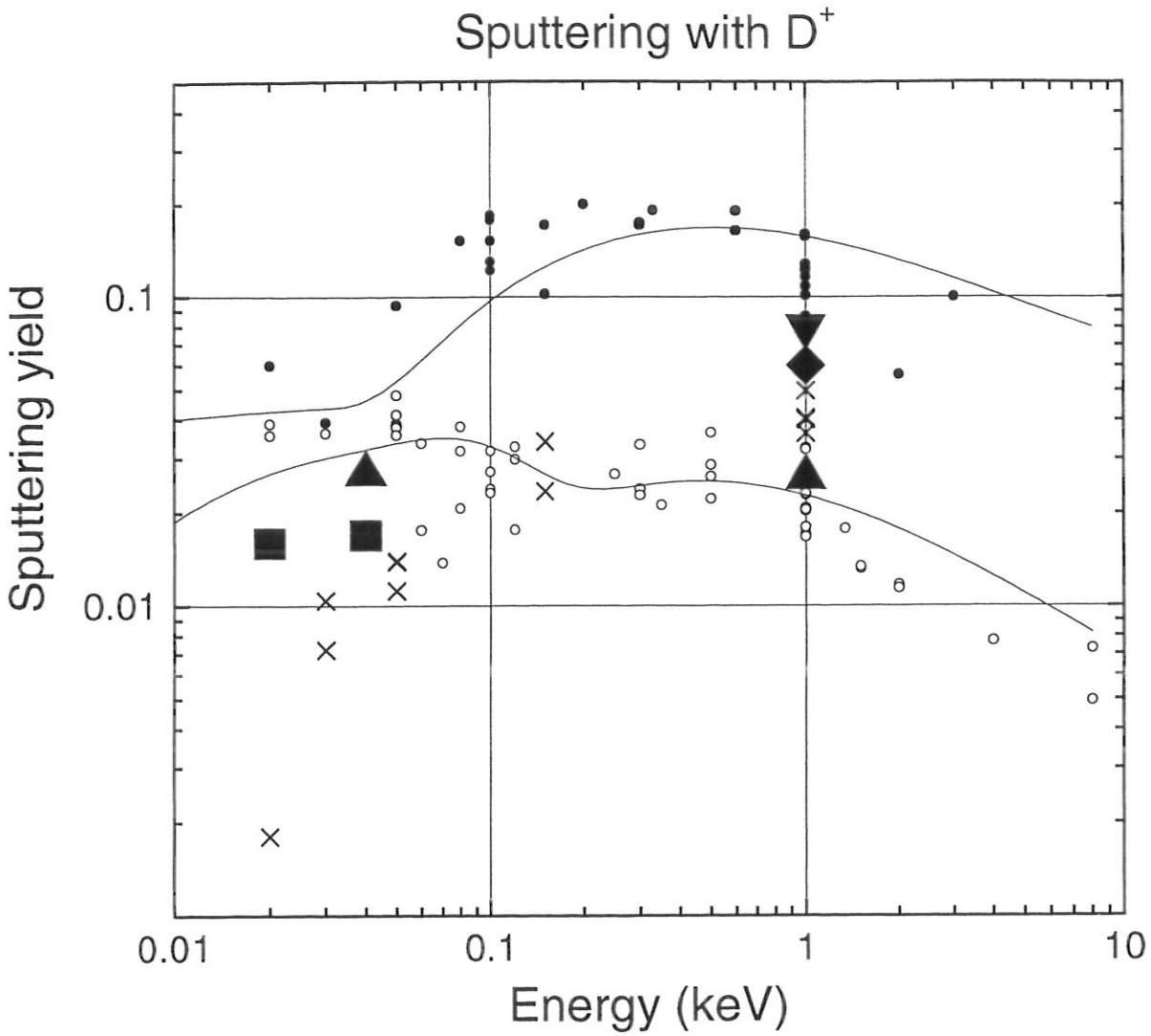
Sputtering with D+
Sputtering yield
0.1
0.01
0.01
0.1
1
10
Energy (keV)

FIGURE 13

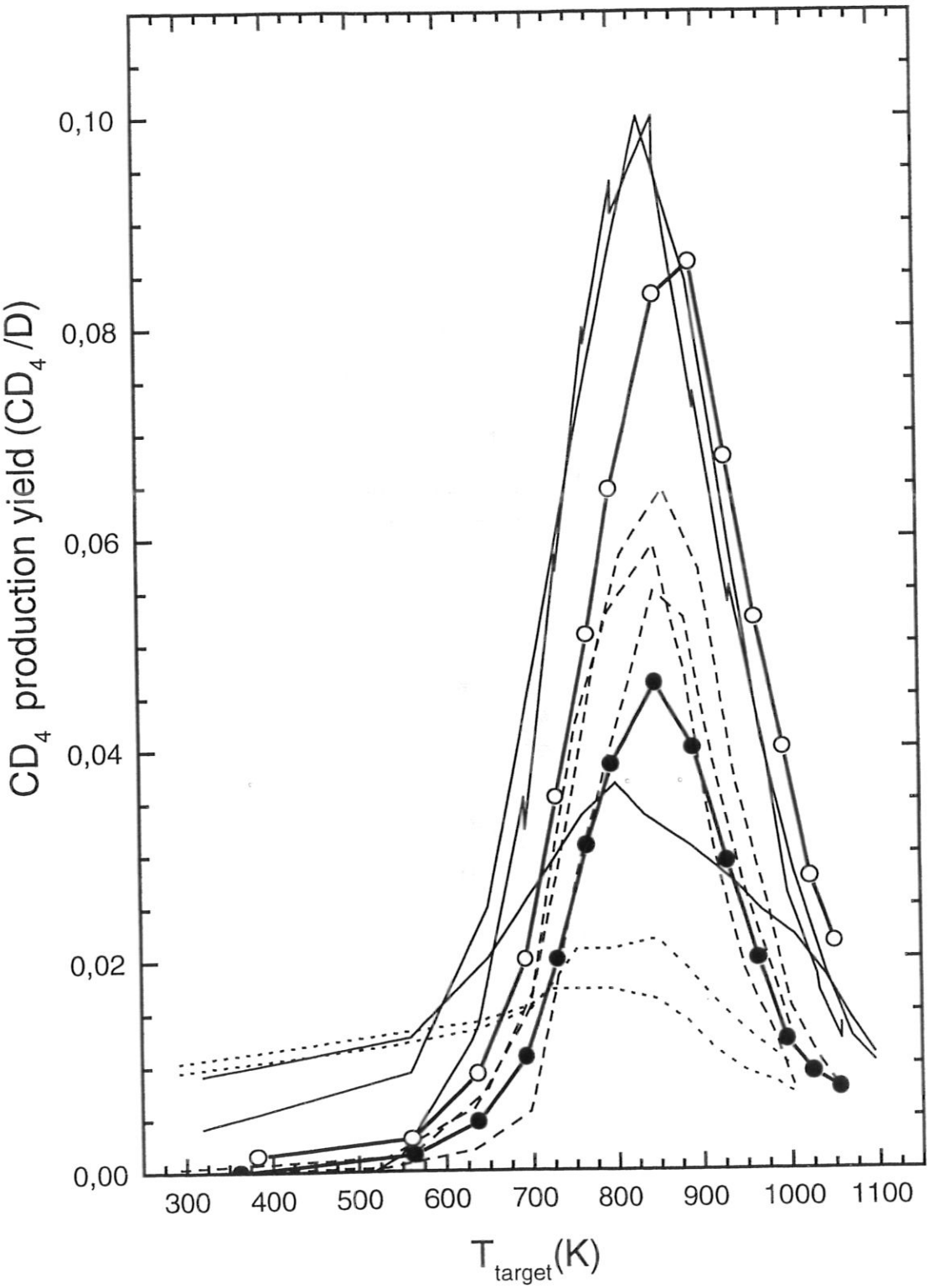
0,10
0,08
0,06
0,04
0,02
0,00
CD4 production yield (CD4 /D)
300
400
500
600
700
800
900
1000
1100
Ttarget(K)

FIGURE 14

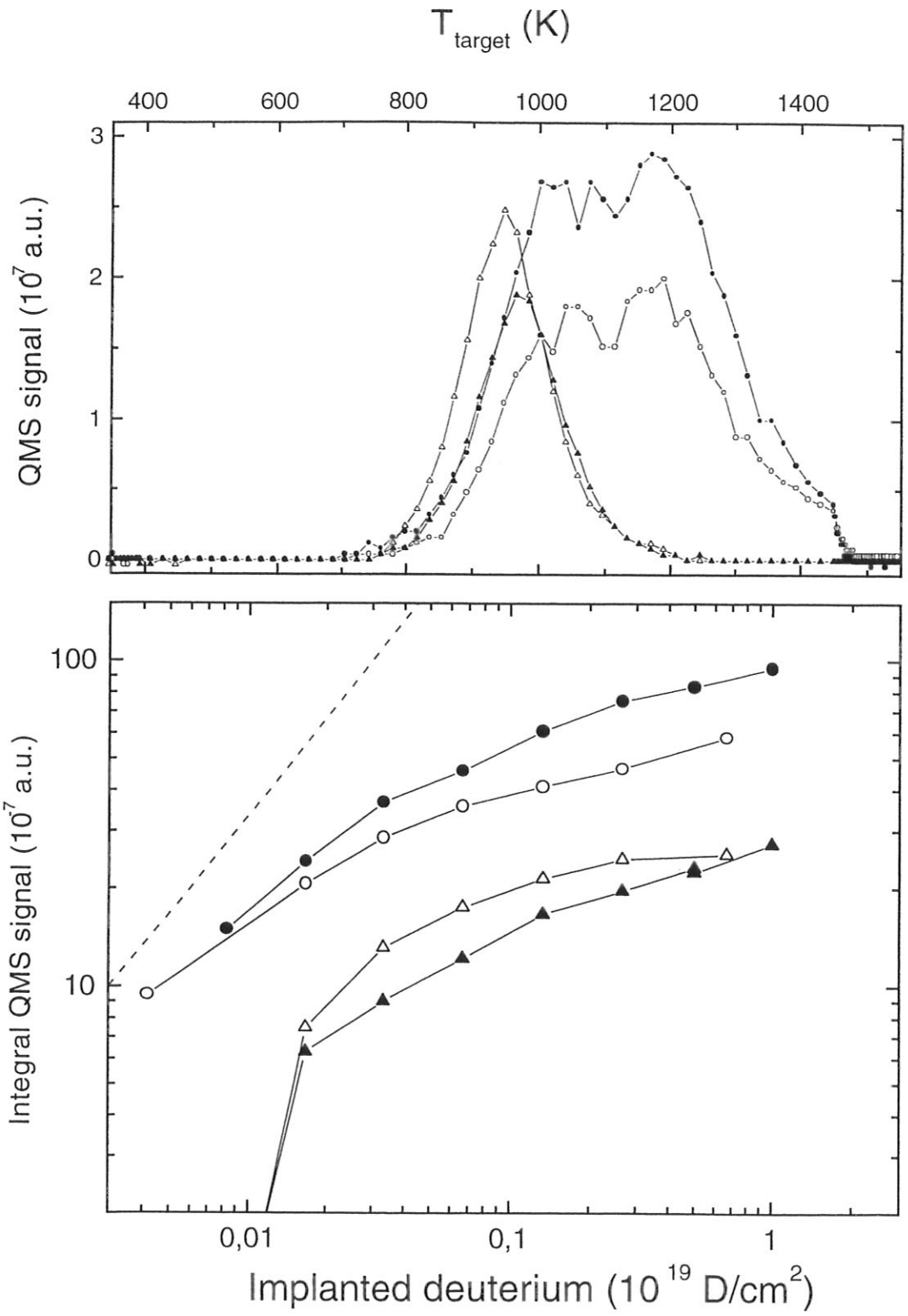
T target (K)
400
600
800
1000
1200
1400
QMS signal (10^7 a.u.)
3
2
1
0
Integral QMS signal (10^7 a.u.)
100
10
0,01
0,1
1
Implanted deuterium (10^19 D/cm^2)

FIGURE 15